Comput. Methods Appl. Mech. Engrg. 225–228 (2012) 55–64

Contents lists available at SciVerse ScienceDirect

Comput. Methods Appl. Mech. Engrg.

journal homepage: www.elsevier.com/locate/cma

A nonlocal plasticity formulation for the material point method

J. Burghardt [a,*], R. Brannon [a], J. Guilkey [b]

[a] University of Utah, 50 S. Campus Dr., Salt Lake City, UT 84112, USA
[b] Schlumberger-Perforating Research, 1935 South Fremont Drive, Salt Lake City, UT 84104, USA

ARTICLE INFO

Article history:
Received 24 June 2011
Received in revised form 8 February 2012
Accepted 8 March 2012
Available online 17 March 2012

Keywords:
Nonlocal plasticity
Material point method
Localization
Integral equations
Fixed-point iteration

ABSTRACT

A new multi-variate fixed-point iteration scheme is devised for solving the coupled dynamic integral equations governing nonlocal plasticity using the material point method (MPM). Novel use of the MPM grid for particle–particle communications results in a simple and efficient, matrix-free method. Moreover, a straightforward method for deriving a convergence criterion for this method is developed and applied to two classical verification problems that are well known to be mesh dependent with a local model, but are shown to be mesh-independent with the new nonlocal MPM formulation.

1. Introduction

The material point method (MPM) is a particle-based method for solving large-deformation solid mechanics problems [1,2]. In this method, the problem domain is discretized into particles that carry material data such as mass, velocity, internal state variables, etc. At each time step, the mass, velocity, and internal force are projected from the particles to a "background" grid, which is typically (though not necessarily) taken to be Eulerian. The equations of motion are solved on the background grid, and the updated velocity and acceleration fields at the grid nodes are then mapped to the particles to update the particle position and velocity, respectively. The updated grid velocity field is used to calculate the velocity gradient, rate of deformation, and updated deformation gradient tensors at each particle, which then may be used by the constitutive model to update the stress at each particle. The MPM equations and algorithm are summarized in Section 2. For a more complete description of the method see Steffen and Wallstedt for a review [3]. An implicit version of the MPM has also been developed [4,5], but only the explicit MPM is considered in this paper.

The material point method has successfully been used to solve a wide variety of solid mechanics problems including fluid–structure interaction [6], finite-deformation plasticity [7], fracture mechanics [8,9], and impact/penetration [10,11]. Many potential areas of application of the MPM involve material softening (i.e., loss of strength due to inelastic deformation). When softening occurs, plastic deformation often localizes into a discrete region, which has been shown to result in a loss of hyperbolicity and ill-posedness of the governing equations [12,13]. The consequence of this ill-posedness, in numerical simulations, is that the localization zone becomes proportional to the mesh spacing. As the mesh is refined, the localization zone therefore becomes ever smaller, and the work to failure after the peak load is reached approaches zero. In a real material, the size of a localization zone would be determined by the length scale of the underlying material micro-structure (grain size, void distribution, etc.). However, local material models possess no intrinsic length scale from which the size of a localization zone can be established.

Spatially nonlocal plasticity theory has been developed to introduce an intrinsic length scale to plasticity models. This intrinsic length scale results in two important characteristics. First it serves as a localization limiter, which restores the well-posedness of the initial boundary-value problem by limiting the width of a localization zone [14–16]. Second, it results in the prediction of a size-effect, which causes the length scale of a structure relative to the material's structure to influence its mechanical response, as has been observed in the laboratory [17,18]. This is in contrast to a traditional local continuum material where no intrinsic length scale is associated with the material, and hence, no size effect is predicted.

Here the term nonlocal is used to describe any type of plasticity model that includes an intrinsic length scale. Two classes of nonlocal models have emerged in the literature: strongly nonlocal and weakly nonlocal. The strongly nonlocal formulations include nonlocal models of the integral type, as well as the implicit gradient model of Engelen and Geers [19,20]. The weakly nonlocal

* Corresponding author.
E-mail addresses: j.burghardt@utah.edu, jeff788@gmail.com (J. Burghardt).

0045-7825/$ - see front matter © 2012 Elsevier B.V. All rights reserved.
http://dx.doi.org/10.1016/j.cma.2012.03.007

models include the explicit gradient models [16,21]. For a comparison of the explicit gradient, implicit gradient, and integral-type nonlocal models see the paper by Peerlings et al. [22]. For a more complete survey of the various nonlocal models that have been developed see the papers by Bažant and Jirásek [23] and Di Luzio and Bazant [24].

In terms of implementation, a local plasticity model results in an uncoupled set of algebraic constitutive equations, whereas nonlocal formulations, when discretized, result in a coupled set of constitutive equations. The integral-type formulation results in a coupled set of integral equations [15,25]. The explicit gradient formulation results in a partial differential equation which must be solved over the plastic portion of the domain [21]. The implicit gradient formulation results in a partial differential equation of the Helmholtz type which must be solved simultaneously with the equations of motion or equilibrium [19]. Various methods have been employed to solve these additional equations. The focus of this paper is solving the equation of the integral-type nonlocal models.

The integral-type nonlocal models have a few distinct advantages and disadvantages as compared to the gradient models. Both the integral-type and implicit gradient models are strongly nonlocal, which makes them effective at limiting the size of localized regions and thereby restoring the well-posedness to localization problems. An advantage of integral-type nonlocal models is that the treatment of nonlocal terms at material boundaries is more transparent and physically meaningful as compared to the physically ambiguous boundary conditions that must be specified with both implicit and explicit gradient models. The primary disadvantage to the integral-type models is the difficulty of solving the resulting system of integral equations. The purpose of this paper is to present a new method of solving this coupled system of integral equations using the material point method (MPM).

The approach taken in this paper is closely related to that used by Stromberg and Ristinmaa with the FEM [25]. The unique contributions of the present work are:

1. Whereas integral-type nonlocal models have been implemented previously using other methods [15,25–28], this is the first paper to present a nonlocal plasticity algorithm for the MPM.
2. A method for evaluating the nonlocal integrals is presented that uses the MPM background grid rather than body-fixed Lagrangian points. This scheme eliminates the need to maintain a list of "neighboring" material points within the support domain of the nonlocal weighting function around each material point. This is particularly important for large deformation problems where the number and identity of the particles within the nonlocal support domain of a particle changes in time.
3. A straightforward method for deriving a convergence criterion for the new method is presented. Stromberg and Ristinmaa demonstrated that their iteration scheme converged for the problems considered in that work, but they did not derive a general convergence criterion. In the present work, we show that a similar iteration scheme may be derived using a multivariate fixed-point iteration scheme. Using a Drucker–Prager yield model, Section 4 summarizes various fixed-point systems that can be derived from the same set the yield equations. The Banach contraction mapping theorem is used to derive a general convergence criterion for two of these possible iteration schemes for the Drucker–Prager model. The resulting convergence criteria reveal under what conditions each fixed-point formulation is preferred.

The organization of the paper is as follows. Section 2 is a brief overview of the MPM. Section 3 provides an overview of the equations of nonlocal plasticity. In Section 4 we derive two fixed-point iteration schemes for a nonlocal Drucker–Prager plasticity model. Section 5 discusses the implementation of the fixed-point iteration scheme within the MPM. Finally, in Section 6, results are presented from two simple localization problems. The nonlocal plasticity method presented here is shown to cause the localization zone to converge to a finite width as the mesh is refined. The width of the localization region is shown to be proportional to the nonlocal length scale parameter. Additionally, the behavior of a structure is shown to depend upon the ratio of the specimen length scale and the nonlocal length scale.

2. Review of the material point method

With the material point method (MPM), the problem domain is discretized into a set of Lagrangian material point particles. Each MPM particle represents a finite Lagrangian volume of the material, and is used to track the properties of that volume (e.g., mass m_p, volume V_p, density $\rho_p = m_p/V_p$, stress $\boldsymbol{\sigma}_p$, deformation gradient tensor $\boldsymbol{F}_p$, internal variables, etc.). The method also makes use of a "background" grid. Though it is not required by the method, a uniform, structured Eulerian background grid is often used. Using an Eulerian grid is equivalent to resetting the grid at the end of each time step and treating the "reset" grid as the kinematic reference configuration for each time step. In this way the kinematic approach of the MPM is essentially equivalent to that of the updated Lagrangian finite-element method. For each time step, the equations of motion are solved on the background grid in the same manner as with the finite element method (FEM). Accordingly, the lumped mass array is given by

$$m_i = \int_\Omega \rho(\boldsymbol{x}) S_i(\boldsymbol{x}) dV, \tag{1}$$

where ρ is the mass density, and S_i is the shape function associated with the i^{th} grid node. With the FEM, the integral in Eq. (1) is broken up, without loss, into a sum of integrals over element domains. With the MPM, on the other hand, the integral in Eq. (1) is broken up into a sum of integrals over non-overlapping particle domains Ω_p:

$$m_i = \sum_p \rho_p \int_{\Omega_p} S_i(\boldsymbol{x}) dV, \tag{2}$$

where ρ_p is the density of the p^{th} particle, which is assumed to be constant over the particle domain. Similarly, the internal force array is

$$\boldsymbol{f}_i^{\text{int}} = -\sum_p \boldsymbol{\sigma}_p \cdot \int_{\Omega_p} \nabla S_i(\boldsymbol{x}) dV. \tag{3}$$

In principle, each integral over the particle domain may be evaluated exactly if Ω_p is treated as the Voronoi cell for the particle. To avoid the need for finding the Voronoi tessellation, these integrals may be approximated as follows:

$$m_i = \sum_p m_p \phi_{ip} \tag{4}$$

and

$$\boldsymbol{f}_i = \sum_p \boldsymbol{\sigma}_p \cdot \boldsymbol{G}_{ip}, \tag{5}$$

where

$$\phi_{ip} = \frac{1}{V_p^*} \int_{\Omega^*} S_i^*(\boldsymbol{x}) \chi_p(\boldsymbol{x}) dV, \tag{6}$$

$$\boldsymbol{G}_{ip} = \frac{1}{V_p^*} \int_{\Omega^*} \nabla S_i^*(\boldsymbol{x}) \chi_p(\boldsymbol{x}) dV \tag{7}$$

and

$$V_p^* = \int_{\Omega^*} \chi_p(\boldsymbol{x}) dV. \tag{8}$$

Eqs. (6) and (7) have introduced a generalized integration domain Ω^*, as well as a weight function $\chi_p(\boldsymbol{x})$, and possibly an alternative shape function to allow these integrals to reduce to the various MPM formulations in the literature. If $S_i^*(\boldsymbol{x}) = S_i(\boldsymbol{x}),\ \Omega^* = \Omega_p$, and χ_p is the Dirac delta function, then the result is the standard MPM formulation [1]. If $S_i^*(\boldsymbol{x}) = S_i(\boldsymbol{x}),\ \Omega^* = \Omega_u$, with $\chi_p = 1$ on Ω_u and 0 elsewhere, where Ω_u is an nondeforming cuboid, then the result is the "uGIMP" formulation [2]. Finally, if $S_i^*(\boldsymbol{x}) = S_i^{app}(\boldsymbol{x})$, where $S_i^{app}(\boldsymbol{x})$ is a linear interpolating function across the generalized domain $\Omega^* = \Omega_{CPDI}$, and $\chi_p = 1$ on Ω_{CPDI} and 0 elsewhere, where Ω_{CPDI} is a parallelepiped that deforms with the particle's deformation gradient, then the result is the CPDI formulation [29]. For a quantitative comparison of the error of standard MPM and GIMP, see the paper by Wallstedt and Guilkey [30], and for a comparison of GIMP and CPDI see the paper by Sadeghirad et al. [29]. Additionally, an improved velocity projection method has been developed by Wallstedt and Guilkey [31], but is not considered in the present work.

Regardless of the MPM formulation that is used, the internal force vector, along with any external force vector f_i^{ext}, and the lumped mass m_i are used to solve for the nodal acceleration vector:

$$\boldsymbol{a}_i = \frac{\boldsymbol{f}_i^{int} + \boldsymbol{f}_i^{ext}}{m_i}. \tag{9}$$

The updated grid velocities $\boldsymbol{v}_i$, are found using an explicit forward-Euler time integration scheme:

$$\boldsymbol{v}_i^{n+1} = \boldsymbol{v}_i^n + \boldsymbol{a}_i \Delta t. \tag{10}$$

The velocity gradient at each particle is calculated using:

$$\nabla \boldsymbol{v}_p^{n+1} = \sum_i \boldsymbol{G}_{ip} \boldsymbol{v}_i^{n+1}. \tag{11}$$

The deformation gradient tensor is then update using:

$$\boldsymbol{F}^{n+1} = \boldsymbol{F}^n (\nabla \boldsymbol{v}_p^{n+1} + \boldsymbol{I}). \tag{12}$$

The polar decomposition of $\boldsymbol{F}^n$ and $\boldsymbol{F}^{n+1}$ is used to find the material rotation tensor at the beginning and end of the step. To satisfy frame indifference, the symmetric part of the velocity gradient and the stress tensor at the beginning of the step are both unrotated prior to calling the constitutive model. After the constitutive model computes the updated stress tensor, it is re-rotated using the material rotation tensor at the end of the time step.

The symmetric part of the velocity gradient tensor is then used to update the stress state of each particle. Finally, the particle position, velocity are updated according to:

$$\boldsymbol{x}_p = \boldsymbol{x}_p^n + \sum_i \phi_{ip} \boldsymbol{v}_i \Delta t \tag{13}$$

and

$$\boldsymbol{v}_p = \boldsymbol{v}_p^n + \sum_i \phi_{ip} \boldsymbol{a}_i \Delta t, \tag{14}$$

respectively.

As mentioned, all problem data (density, stress, etc.) are saved at particles. Accordingly, the continuous approximation to any field $h(\boldsymbol{x})$ is then described on the background grid as

$$h(\boldsymbol{x}) = \sum_i h_i S_i(\boldsymbol{x}), \tag{15}$$

where h_i is the nodal value on the grid, calculated from particle values, h_p, by

$$h_i = \frac{1}{m_i} \sum_p \phi_{ip} h_p m_p. \tag{16}$$

The MPM formally belongs to the class of meshless methods for which fields are described by

$$h(\boldsymbol{x}) = \sum_p h_p B_p(\boldsymbol{x}) \tag{17}$$

in which $B_p(\boldsymbol{x})$ are particle basis functions. The computational advantage of the MPM is that these particle basis functions do not need to be constructed explicitly. In particular, substituting Eq. (16) into (15) shows that the MPM particle basis functions are

$$B_p(\boldsymbol{x}) = \sum_i \frac{m_p}{m_i} \phi_{ip} S_i(\boldsymbol{x}). \tag{18}$$

3. Nonlocal plasticity

In nonlocal plasticity theory, as in classical elastoplasticity theory, the strain rate $\dot{\boldsymbol{\epsilon}}$ is assumed to be additively decomposed into elastic and plastic parts, $\dot{\boldsymbol{\epsilon}}^e$ and $\dot{\boldsymbol{\epsilon}}^p$, respectively:

$$\dot{\boldsymbol{\epsilon}} = \dot{\boldsymbol{\epsilon}}^e + \dot{\boldsymbol{\epsilon}}^p. \tag{19}$$

The stress rate tensor $\dot{\boldsymbol{\sigma}}$ is given by elasticity theory according to

$$\dot{\boldsymbol{\sigma}} = \mathbb{C} : \dot{\boldsymbol{\epsilon}}^e, \tag{20}$$

where $\mathbb{C}$ is the fourth-order elastic tangent stiffness tensor. The plastic strain rate is described by the flow rule according to Eq. (21):

$$\dot{\boldsymbol{\epsilon}}^p = \dot{\lambda} \widehat{\boldsymbol{M}}; \tag{21}$$

where $\dot{\lambda}$ is the "rate-like" plastic multiplier and $\widehat{\boldsymbol{M}}$ is a unit tensor defining the direction of the plastic strain rate tensor.

Bazant and Lin's nonlocal plasticity model included a nonlocal average of the plastic strain rate tensor in the strain rate decomposition equation [15]. In that seminal work, every occurrence of the plastic strain rate tensor in classical theory was replaced with a nonlocal average. Subsequent work demonstrated that this is not necessary (and, in some cases, not sufficient) to regularize the governing equations [25,24]. Specifically, nonlocal terms are needed only in the evolution equations for the internal state variables that drive softening.

As in classical plasticity, the yield function f is a scalar function of the stress tensor and a set of internal state variables that change in response plastic loading. Each internal state variable may either be a local or nonlocal variable. For simplicity, only one local internal state variable, η, and one nonlocal internal state variable, ζ, will be considered. Extension of the theory to account for any number of local or nonlocal internal state variables should be self-evident.

The standard Karush–Kuhn–Tucker plastic complementarity conditions are:

$$f\dot{\lambda} = 0, \quad f \leqslant 0, \quad \dot{\lambda} \geqslant 0. \tag{22}$$

These equations may equivalently be written as (c.f. [25]):

$$f = w, \quad w\dot{\lambda} = 0, \quad w \leqslant 0, \quad f \leqslant 0, \quad \dot{\lambda} \geqslant 0. \tag{23}$$

where w is a so-called "slack" variable. The solution to the complementarity problem consists of finding w and $\dot{\lambda}$, at least one of which must be zero, at each material point. In practical terms, this involves determining which particles are undergoing plastic deformation in a given time step, and determining the value of $\dot{\lambda}$ during that step. If $w < 0$, the actual value of w is not of interest.

Although within the plasticity community Eq. (23) is an uncommon way of expressing the plastic complimentarity condition, this form highlights the fact that determining which particles are undergoing plastic deformation is an important part of the solution procedure. For a local model this involves only checking the sign of the yield function. As will be shown, for a nonlocal model, making this determination is not so trivial. The complementarity form of the consistency equation also results in a more straightforward

means of expressing the iteration scheme described in the next section.

The local internal state variable η evolves according to

$$\dot{\eta} = h_\eta \dot{\lambda}, \tag{24}$$

where h_η is the local hardening/softening modulus. The nonlocal internal state variable ζ evolves according to

$$\dot{\zeta} = h_\zeta \langle \dot{\lambda} \rangle, \tag{25}$$

where h_ζ is the nonlocal hardening/softening modulus, and $\langle \cdot \rangle$ is the nonlocal averaging operator defined by a weighted average integral over the entire problem domain Ω:

$$\langle \dot{\lambda} \rangle = \frac{1}{V_\beta} \int_\Omega \beta(\boldsymbol{x} - \boldsymbol{s}) \dot{\lambda}(\boldsymbol{s}) d\boldsymbol{s}. \tag{26}$$

Here, $\boldsymbol{x}$ is the location of a given particle and $\beta(\boldsymbol{x})$ is the nonlocal weighting function, and

$$V_\beta = \int_\Omega \beta(\boldsymbol{x} - \boldsymbol{s}) d\boldsymbol{s}. \tag{27}$$

The divisor V_β normalizes the nonlocal average, and also serves an important role at boundaries. The internal state variables η and ζ are generally initialized to zero, which is equivalent to assuming that the material is in a virgin state, or at least in the same state as the material used to calibrate the constitutive model. The weighting function of a particle that is adjacent to a material boundary will have a portion of its support outside of Ω. This portion of the weighting function will not contribute to V_β, thus reducing the value of V_β compared to that of an interior particle. In this way the amplitude of the weighting function near a boundary is increased so that the nonlocal averaging remains normalized despite the truncation of the portion of the weighting function that extends beyond the boundary. Whereas gradient-type models require setting boundary conditions on the plastic strain field, this is the only special treatment of the boundaries that is necessary with an integral-type model.

A truncated Gaussian bell-curve is used for the nonlocal weighting function:

$$\beta(\boldsymbol{x}) = \mathrm{Exp}[-(k\|\boldsymbol{x}\|/l)^2], \quad 0 \leqslant \|\boldsymbol{x}\| \leqslant l \beta(\boldsymbol{x}) = 0, \quad \|\boldsymbol{x}\| > l, \tag{28}$$

where $k = (6\sqrt{\pi})^{\frac{1}{3}}$ for a 3D simulation, 2 for a 2D simulation, $\sqrt{\pi}$ for a 1D simulation, and l is the nonlocal length scale. This choice for the nonlocal weighting function is not unique. The critical properties of the weighting function are the extent of the function's support, and the smoothness. It has been reported in the literature that a smooth weighting function results in a higher rate of convergence [15].

The generalized nonlocal model described here allows for both local and nonlocal hardening/softening. If h_η were zero, the result would be a purely nonlocal model, and if h_ζ were zero, a purely local model is recovered. Several studies in the literature advocate using both local and nonlocal terms [25,32,24]. Stromberg and Ristinmaa's model of this type, which was called an overlocal model by Di Luzio and Bazant [24], is obtained by letting $h_\eta > 0$ and $h_\zeta < 0$. If each internal variable is defined such that an increase in the internal variable tends to increase the yield strength, then an overlocal model corresponds to local contributions to hardening and nonlocal contributions to softening.

If a backward Euler implicit integration scheme is used for updating $\boldsymbol{\sigma}, \eta$, and ζ, the first equation in (23) may be written at the end of time step k as

$$f\left(\boldsymbol{\sigma}^n + \dot{\boldsymbol{\sigma}}^{n+1}\Delta t, \eta^n + h_\eta \dot{\lambda}^{n+1}\Delta t, \zeta^n + h_\zeta \langle \dot{\lambda} \rangle^{n+1}\Delta t\right) = w^{n+1}, \tag{29}$$

where the superscripted n refers to the time step number. In general the hardening moduli can change during plastic loading increments, but are often simply taken to be constant over a time step. Eqs. (19)–(21) can be combined to give:

$$\dot{\boldsymbol{\sigma}} = \mathbb{C} : \dot{\boldsymbol{\epsilon}} - \dot{\lambda}\boldsymbol{A}; \tag{30}$$

where $\boldsymbol{A} = \mathbb{C} : \widehat{\boldsymbol{M}}$. Substituting Eq. (30) into Eq. (29) gives

$$f(\boldsymbol{\sigma}_{\mathrm{trial}} - \Delta\lambda^{n+1}\boldsymbol{A}^{n+1}, \eta^{n+1}, \zeta^{n+1}) = w^{n+1}, \tag{31}$$

where

$$\eta^{n+1} = \eta^n + h_\eta \dot{\lambda}^{n+1}\Delta t, \tag{32}$$

$$\zeta^{n+1} = \zeta^n + h_\zeta \langle \dot{\lambda} \rangle^{n+1}\Delta t \tag{33}$$

and

$$\boldsymbol{\sigma}_{\mathrm{trial}} = \boldsymbol{\sigma}^n + \mathbb{C} : \dot{\boldsymbol{\epsilon}}^{n+1}\Delta t. \tag{34}$$

The objective of the nonlocal plasticity algorithm is to find the fields $\dot{\lambda}^{n+1}$, and w^{n+1}, that satisfy Eq. (31), ensuring that the plastic consistency condition is satisfied at each time step.

4. Fixed-point iteration scheme for linear Drucker–Prager yield function

For simplicity, we restrict the discussion to a linear Drucker–Prager yield function with linear isotropic hardening/softening. The discretization method used here may nevertheless be used for any yield function desired. The Drucker–Prager yield function is:

$$f(\boldsymbol{\sigma}, \eta, \zeta) = \sqrt{J_2} + \alpha I_1 - k_o - \eta - \zeta, \tag{35}$$

where $J_2 = \frac{1}{2}\boldsymbol{S} : \boldsymbol{S}, \boldsymbol{S}$ is the deviatoric stress tensor, and $I_1 = \mathrm{Tr}(\boldsymbol{\sigma})$. The material parameters are α, and k_o. These parameters are proportional to the friction angle and cohesion, respectively. The direction of the plastic strain rate tensor is prescribed to be proportional to the unit normal to the plastic flow potential surface. The plastic flow potential is taken to have the same functional form as the yield function. The only material parameter affecting the direction of the plastic strain rate tensor is the dilatation parameter α_p. The dilatation angle controls the ratio of volumetric to deviatoric plastic strain. If α_p is chosen to coincide with α, then the plastic potential and the yield surface are identical, which is called an associated model. The plastic flow direction is then

$$\widehat{\boldsymbol{M}} = \frac{\frac{1}{\sqrt{2}}\frac{\boldsymbol{S}^{n+1}}{\|\boldsymbol{S}^{n+1}\|} + \alpha_p \boldsymbol{I}}{\sqrt{\frac{1}{2} + 3\alpha_p^2}}, \tag{36}$$

where, consistent with the backward-Euler scheme, $\boldsymbol{S}^{n+1}$ is the deviatoric stress tensor at the end of the time step, and $\boldsymbol{I}$ is the second-order identity tensor. Using the yield function in (35), and substituting these expressions into Eq. (31) for plastic particles ($w = 0$) under the additional assumption that the elastic stiffness is constant and isotropic, the yield function at the end of the step evaluates to

$$f(\boldsymbol{\sigma}_{\mathrm{trial}} - \Delta\lambda\boldsymbol{A}, \eta^{n+1}, \zeta^{n+1}) = f_{\mathrm{trial}} - \Delta\lambda\frac{G}{\sqrt{\frac{1}{2} + 3\alpha_p^2}} - \Delta\lambda\frac{9\alpha K\alpha_p}{\sqrt{\frac{1}{2} + 3\alpha_p^2}} - h_\eta\Delta\lambda - h_\zeta\langle\Delta\lambda\rangle = 0, \tag{37}$$

where G is the shear modulus, K is the bulk modulus, $\Delta\lambda = \dot{\lambda}\Delta t$, and

$$f_{\mathrm{trial}} = f(\boldsymbol{\sigma}_{\mathrm{trial}}, \eta^n, \zeta^n). \tag{38}$$

Since $\langle\Delta\lambda\rangle$ is an integral operator that includes contributions from other particles, Eq. (37) gives a coupled system of integral equations to be satisfied at each plastic particle. The new technique presented in this paper solves this system by first transforming it into an equivalent system of fixed-point equations.

There are several ways of transforming Eq. (37) into a system of fixed-point equations, some resulting in better convergence behavior than others. In most cases, convergence depends upon the selected material parameters. To illustrate this point, two fixed-point expressions of Eq. (37) are examined. These two choices are not unique, and many of the possible choices of fixed-point formulas may not converge for any choice of initial conditions or material parameters. Despite the multitude of choices for setting up the fixed-point system, there are some basic guidelines for wisely choosing a fixed-point system. These guidelines will be discussed below by appealing to the convergence criteria for the two example methods presented here. The first is generated by taking all local values of $\Delta\lambda$ to be the updated value, with the nonlocal term being evaluated using the previous estimate for $\Delta\lambda$. This gives

$$f_{\text{trial}} - \Delta\lambda^{k+1}\frac{G}{\sqrt{\frac{1}{2}+3\alpha_p^2}} - \Delta\lambda^{k+1}\frac{9\alpha K\alpha_p}{\sqrt{\frac{1}{2}+3\alpha_p^2}} - h_\eta\Delta\lambda^{k+1} - h_\zeta\langle\Delta\lambda^k\rangle = 0, \tag{39}$$

where k is the iteration number. Solving this expression for $\Delta\lambda^{k+1}$ gives

$$\Delta\lambda^{k+1} = \frac{f_{\text{trial}} - h_\zeta\langle\Delta\lambda^k\rangle}{\frac{G}{\sqrt{\frac{1}{2}+3\alpha_p^2}} + \frac{9\alpha K\alpha_p}{\sqrt{\frac{1}{2}+3\alpha_p^2}} + h_\eta}. \tag{40}$$

The other fixed-point equation considered is the same as that in Eq. (40) except that the local hardening term (i.e., coefficient of h_η) is evaluated using the previous estimate for $\Delta\lambda$:

$$f_{\text{trial}} - \Delta\lambda^{k+1}\frac{G}{\sqrt{\frac{1}{2}+3\alpha_p^2}} - \Delta\lambda^{k+1}\frac{9\alpha K\alpha_p}{\sqrt{\frac{1}{2}+3\alpha_p^2}} - h_\eta\Delta\lambda^{k} - h_\zeta\langle\Delta\lambda^k\rangle = 0. \tag{41}$$

The resulting fixed-point equation is

$$\Delta\lambda^{k+1} = \frac{f_{\text{trial}} - h_\eta\Delta\lambda^k - h_\zeta\langle\Delta\lambda^k\rangle}{\frac{G}{\sqrt{\frac{1}{2}+3\alpha_p^2}} + \frac{9\alpha K\alpha_p}{\sqrt{\frac{1}{2}+3\alpha_p^2}}}. \tag{42}$$

The convergence criterion for each of these fixed-point schemes is found by computing the derivative of $\Delta\lambda^{k+1}$ with respect to $\Delta\lambda^k$. Applying the Banach fixed-point theorem, this fixed-point scheme will converge to a unique fixed-point if

$$\mathscr{L} = N_\beta\left\|\frac{\partial\Delta\lambda^{k+1}}{\partial\Delta\lambda^k}\right\| < 1, \tag{43}$$

where N_β is the number of particles within the support of $\beta(\boldsymbol{x})$. $\mathscr{L}$ is called the Lipschitz constant of the system of equations. The Lipschitz constant for the first iteration scheme is bounded by

$$\mathscr{L}_1 \leqslant N_\beta\left\|\frac{h_\zeta}{\frac{G}{\sqrt{\frac{1}{2}+3\alpha_p^2}} + \frac{9\alpha K\alpha_p}{\sqrt{\frac{1}{2}+3\alpha_p^2}} + h_\eta}\right\|, \tag{44}$$

where, referring to Eq. (26), use has been made of the fact that

$$\begin{aligned}\frac{\partial\langle\Delta\lambda_i\rangle}{\partial\Delta\lambda_j} &= \frac{\partial}{\partial\Delta\lambda_j}\frac{1}{V_\beta}\sum_n\Delta\lambda_n\beta(\boldsymbol{x}_p-\boldsymbol{x}_n) = \frac{1}{V_\beta}\sum_n\frac{\partial\Delta\lambda_n}{\partial\Delta\lambda_j}\beta(\boldsymbol{x}_p-\boldsymbol{x}_n)\\ &= \frac{1}{V_\beta}\sum_n\delta_{nj}\beta(\boldsymbol{x}_p-\boldsymbol{x}_n) = \frac{1}{V_\beta}\beta(\boldsymbol{x}_p-\boldsymbol{x}_j) \leqslant 1,\end{aligned} \tag{45}$$

where δ_{nj} is the Kroneker delta. Similarly the Lipschitz constant for the second fixed-point scheme is bounded by:

$$\mathscr{L}_2 \leqslant N_\beta\left\|\frac{h_\eta + h_\zeta}{\frac{G}{\sqrt{\frac{1}{2}+3\alpha_p^2}} + \frac{9\alpha K\alpha_p}{\sqrt{\frac{1}{2}+3\alpha_p^2}}}\right\|. \tag{46}$$

By comparing Eqs. (44) and (46) some observations can be made regarding how to wisely choose the most effective fixed-point system for a given yield function. In the derivation of Eq. (40) all occurrences of $\Delta\lambda$ except the occurrence in the nonlocal average were taken to be the new estimate for $\Delta\lambda$, whereas in the derivation of Eq. (42) the local hardening term was taken to be the previous estimate for $\Delta\lambda$. The result was that Eq. (40) has a more generous convergence domain than does Eq. (42). Therefore, a general guideline in converting a yield function to a fixed-point system is to take as many occurrences of $\Delta\lambda$ as possible to be the updated value. In general, the more occurrences of $\Delta\lambda$ that are taken to be the updated value, the smaller the Lipschitz constant of the resulting fixed-point system will be.

Smaller values of the Lipschitz constant correspond to faster convergence to the fixed point. Notice that for the local case ($h_\zeta = 0$) the Lipschitz constant for the first scheme is zero, indicating that the scheme will converge to the exact solution in one step. This is to be expected since purely local linear hardening/softening corresponds to a single uncoupled linear equation. For a nonlocal or overlocal model, the rate of convergence depends upon the material parameters ($h_\eta, h_\zeta, G, K, \alpha$ and α_p), as well as the number of particles within the support of the nonlocal weighting function (N_β). With the MPM it is generally a good practice to keep the number of particles per cell constant as the mesh is refined [30]. However, this practice leads to an increase in N_β as the mesh is refined, resulting in a reduction in the convergence rate. Of course, if the Lipschitz constant becomes greater than unity, the fixed-point scheme may diverge. Therefore, for materials for which the softening modulus is large enough to produce a Lipschitz constant greater than one, this fixed-point iteration scheme may not be suitable. However, as will be demonstrated with the first case study problem in Section 6, the structural response may become brittle as a result of either a large softening modulus, or as a result of the structure's length scale being much larger than the length scale of the material's micro-structure. Thus a structure may behave in a very brittle manner without necessarily requiring a large softening modulus.

For nonlinear hardening/softening it would not generally be possible to algebraically transform the yield condition into a fixed-point system. While not demonstrated here, the same general procedure may nevertheless be used, but instead of algebraically solving the yield equation for $\Delta\lambda^{k+1}$, a Newton iteration scheme can be used to generate a fixed-point equation. Stromberg and Ristinmaa's algorithm [25] is a special case of this method. In this case a convergence criterion can be derived in the same way as when the fixed-point equations are algebraically derived. Such a scheme is a nonlinear generalization of the Gauss–Seidel method. A detailed discussion of such schemes can be found in a text by Ortega and Rheinboldt [33].

5. Solution strategy for the MPM

This section describes how the fixed-point iteration scheme presented in the previous section may be incorporated into the MPM. As mentioned in Section 1, the MPM saves field data at particles, and projects the data to grid nodes for solving field equations.

Referring to Eqs. (15) and (16), the standard MPM solution procedure uses particle values of a field, h_p, to construct a grid-based representation of that field, $h(\boldsymbol{x})$. The new nonlocal algorithm presented in this paper is distinguished from other nonlocal solvers in the literature by its use of this MPM mapping to evaluate the nonlocal integrals in the yield equations. As discussed below, this technique makes it unnecessary to build and maintain a list of which particles are involved in the nonlocal average of each particle. An

outline of the algorithm is shown in Algorithm 1, and each step is described in detail below.

The first step in the nonlocal algorithm is to generate an initial estimate for which particles are undergoing plastic deformation, and an initial estimate for $\Delta\lambda$ at those particles. As is done with traditional local constitutive models, the trial stress is computed using the symmetric part of the velocity gradient, which is given in Eq. (11). If evaluating the yield function with the trial stress results in a negative value of the yield function, the particle is *tentatively* considered to be an elastic particle (i.e., $\dot{\lambda} = 0;\ w \neq 0$). If the trial stress state results in a zero or positive value for the yield function, then the particle is considered to be plastic (i.e., $\dot{\lambda} > 0;\ w = 0$). An initial estimate for the increment of the plastic multiplier is found by neglecting nonlocal effects and using a backward Euler integration scheme [34]. Using Eq. (16), the estimate for the plastic multiplier increment is then projected to the grid nodes as

$$\Delta\lambda_i = \frac{1}{m_i}\sum_p \phi_{ip}\Delta\lambda_p m_p, \tag{47}$$

Once the initial estimate for the plastic multiplier increment has been projected to the grid nodes, the initialization for the iterative scheme is complete.

Step two of the nonlocal algorithm is the main iteration loop. For each iteration, the nonlocal integral is evaluated for each plastic particle. This is done by first identifying which grid nodes are within the support domain of the nonlocal weighting function $\beta(\boldsymbol{x})$. Then, the incremental form of the nonlocal integral in Eq. (26) is approximated by a discrete sum using

$$\langle\Delta\lambda\rangle_p = \frac{1}{M_\beta}\sum_i \beta(\boldsymbol{x}_p - \boldsymbol{x}_i)\Delta\lambda_i m_i \tag{48}$$

and

$$M_\beta = \sum_{i=0}^{N_\beta}\beta(\boldsymbol{x}_p - \boldsymbol{x}_i)m_i. \tag{49}$$

By using the nodal mass m_i in the integral, nodes that lie outside of a material boundary are automatically excluded from the sum since $m_i = 0$ for such nodes.

Once the nonlocal integral has been evaluated for a given plastic particle, a fixed-point expression, such as any of those discussed in Section 4, can be used to calculate an improved estimate for the local plastic multiplier, $\Delta\lambda_p^{k+1}$, where k is the iteration number. The nonlocal internal state variables are also updated using backward-Euler time integration of Eq. (25).

During the loop over the particles, the estimate from the previous iteration $\Delta\lambda_p^k$ can be removed from the grid nodes using

$$\Delta\lambda_i \leftarrow \Delta\lambda_i - \frac{m_p}{m_i}\phi_{ip}\Delta\lambda_p^k \tag{50}$$

for each grid node that receives information from the particle. The updated value of $\Delta\lambda_p$ can then be placed on these grid nodes using

$$\Delta\lambda_i \leftarrow \Delta\lambda_i + \frac{m_p}{m_i}\phi_{ip}\Delta\lambda_p^{k+1}. \tag{51}$$

By immediately replacing $\Delta\lambda_p^k$ with $\Delta\lambda_p^{k+1}$ on the grid nodes, all remaining plastic particles for the iteration will be using the most up-to-date data, making the scheme a Gauss–Seidel iteration rather than a Jacobi iteration.

After each loop over the plastic particles, if the maximum value of $|\ \Delta\lambda_p^{k+1} - \Delta\lambda_p^k\ |$ is less than some specified tolerance, the solution is considered converged and the iteration scheme is terminated.

After a converged solution for the field of plastic multipliers has been computed, the nonlocal internal state variables must be updated for the *elastic* particles as well. This is due to the unique feature of nonlocal models that allows plastic deformation at a given particle to change the state of another particle a finite distance away, even if that particle is not undergoing plastic deformation itself. This phenomenon is called plastic diffusion. This also introduces the possibility that the yield surface of a particle that was initially considered to be elastic will contract due to plastic diffusion such that it begins to undergo plastic deformation. If this occurs, the particle must be reclassified as a plastic particle and the field of plastic multipliers must be recomputed, including the new plastic particle. As discussed in Section 3, this illustrates why nonlocal plasticity is best viewed as a complementarity problem where determining which particles are undergoing plastic deformation is an important nontrivial aspect of the solution.

Algorithm 1: Nonlocal plasticity algorithm for the material point method with a Drucker–Prager yield function

Step 1: Initialization
Initialize $\Delta\lambda_i \leftarrow 0$ at each grid node i.
for each particle p **do**
  Compute trial stress, and evaluate f_{trial} using Eq. (38)
  if $f_{\text{trial}} \geqslant 0$ **then**
    Compute initial guess for $\Delta\lambda_p$ by omitting $\langle\Delta\lambda\rangle_p$ in Eq. (42).
    Project $\Delta\lambda_p$ to the i^{th} grid node using $\Delta\lambda_i \leftarrow \Delta\lambda_i + (m_p/m_i)\phi_{ip}\Delta\lambda_p$
  else
    $\Delta\lambda_p \leftarrow 0$
  end if
end for
Step 2: Main Iteration Loop
Initialize iteration counter: $k \leftarrow 0$
while ERROR > TOLERANCE **do**
  $k \leftarrow k + 1$
  for each plastic particle p **do**
    initialize: $\langle\Delta\lambda\rangle_p \leftarrow 0, M_p \leftarrow 0$
    for each node i within nonlocal support domain **do**
      $\langle\Delta\lambda\rangle_p \leftarrow \langle\Delta\lambda\rangle_p + \beta(\boldsymbol{x}_p - \boldsymbol{x}_i)\Delta\lambda_i m_i$
      $M_\beta \leftarrow M_\beta + \beta(\boldsymbol{x}_p - \boldsymbol{x}_i)m_i$
    end for
    $\langle\Delta\lambda\rangle_p \leftarrow \langle\Delta\lambda\rangle_p / M_\beta; \zeta^{n+1} \leftarrow \zeta^n + h_\zeta\langle\Delta\lambda\rangle_p$
    Calculate $\Delta\lambda_p^k$ using Eq. (40) or (42)
    Update stress using Eq. (30)
    Project $\Delta\lambda_p^k$ to the grid nodes using Eqs. (50) and (51).
    $\eta^{n+1} \leftarrow \eta^n + h_\eta\Delta\lambda_p^k$
  end for
  ERROR $\leftarrow \max\left(|\ \Delta\lambda_p^k - \Delta\lambda_p^{k-1}\ |\right)$
end while
Step 3: Evaluate Nonlocal ISVs for elastic particles
for each elastic particle p **do**
  for each node i within nonlocal support domain
    $\langle\Delta\lambda\rangle_p \leftarrow \langle\Delta\lambda\rangle_p + \beta(\boldsymbol{x}_p - \boldsymbol{x}_i)\Delta\lambda_i m_i$
    $M_\beta \leftarrow M_\beta + \beta(\boldsymbol{x}_p - \boldsymbol{x}_i)m_i$
  end for
  $\langle\Delta\lambda\rangle_p \leftarrow \langle\Delta\lambda\rangle_p / M_\beta; \zeta^{n+1} \leftarrow \zeta^n + h_\zeta\langle\Delta\lambda\rangle_p$
  $f_{\text{trial}} \leftarrow f(\boldsymbol{\sigma}_{\text{trial}}, \eta^n, \zeta^{n+1})$
  if $f_{\text{trial}} \geqslant 0$
    Add particle to list of plastic particles
  end if
end for
If the list of plastic particles changed, return to Step 2; otherwise stop.

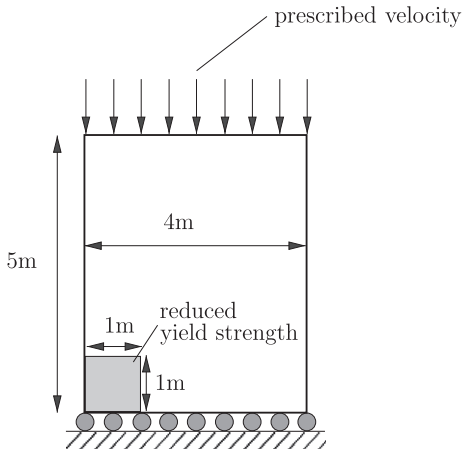

Fig. 1. Schematic of the case study geometry. A symmetric boundary condition is used along the bottom surface, a prescribed velocity boundary condition is used along the top surface, and the lateral faces are stress free. The plate is in a state of plane strain.

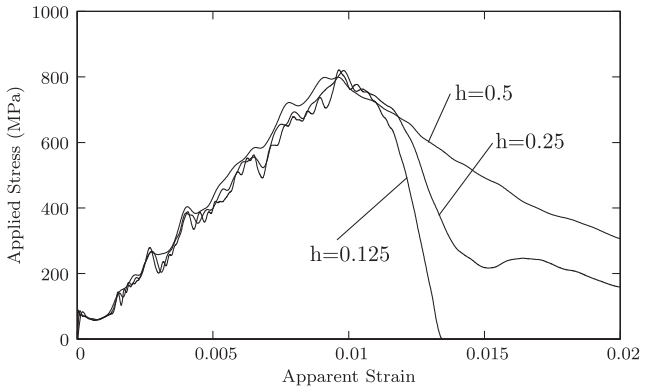

Fig. 3. Non-convergence of applied stress versus apparent axial strain (i.e., % change in plate height) when using a local von Mises plasticity model at three different mesh sizes, h.

6. Numerical examples

In this section, two simple 2D localization problems are solved to illustrate the effectiveness of the nonlocal MPM algorithm just described.

6.1. Axial compression with von Mises plasticity

As illustrated in Fig. 1, this problem consists of 4 m wide and 5 m tall rectangular plane strain plate with a symmetry (i.e., roller) boundary condition at the bottom and a 1 m square region with reduced yield strength at the lower left-hand corner. The top surface of the plate is subject to a prescribed axial velocity, with all other velocity components on that surface set to zero. The lateral surfaces of the plate are traction free.

The bulk modulus is chosen to be 76 GPa, the shear modulus 26 GPa and the yield strength, k_o, was set to 375 MPa in the weakened region, and 400 MPa in the rest of the domain. For both the local and overlocal cases, a von Mises model was used. This is equivalent to setting $\alpha = \alpha_p = 0$ in Eq. (35). This algorithm was implemented into the Uintah explicit dynamics MPM code [35]. This code along with the CPDI interpolation scheme [29] was used to solve the case study problem. Using this interpolation scheme, each particle domain is initially rectangular, and deforms into a parallelogram determined from the deformation gradient of the particle. The prescribed velocity of the top surface was chosen to be 7.5 m/s. Artificial viscosity was used to help dampen out the transient portion of the solution. The time step was chosen to be 20% of the Courant–Friedrichs–Lewy stable time step. For all mesh resolutions used, four material point particles were used in each cell, two in each direction.

The case study problem was first solved using a local von Mises plasticity model with linear softening. The local hardening modulus, h_η, was set to -4.0 GPa, where the negative sign indicates softening. Fig. 2 shows a contour plot of the magnitude of the plastic strain tensor for a mesh spacing, h, of 0.5 m, 0.25 m, and 0.125 m. With all mesh resolutions, a shear band nucleates at the weakened region in the lower left-hand corner of the domain. The anomalous lack of convergence, as seen by the dependence of the shear band width on mesh size, and as further seen in the mesh-dependent post-peak stress–strain response of Fig. 3, is consistent with well-known observations from the literature using other analytical and numerical methods [36,13]. In this case and all others, the applied stress is computed by dividing the total reaction force at the prescribed velocity boundary by the cross-sectional area, assuming unit thickness.

To illustrate the effectiveness of nonlocal theory at eliminating mesh-sensitivity, the axial compression problem was solved using an overlocal von Mises plasticity model using the nonlocal MPM algorithm outlined in Section 5. The local hardening modulus was set to $h_\eta = 2$ GPa, and the nonlocal hardening modulus was set to $h_\zeta = -4$ GPa. This is equivalent to setting Stromberg and Ristinmaa's [25] overlocal parameter to $m = 2$, with the hardening modulus set to $h = -2$ GPa. The nonlocal length scale was set to $L = 0.5$ m. With these values the nonlocal iteration scheme converged in fewer than seven iterations for each time step. Fig. 4 shows contour plots of the magnitude of the plastic strain tensor using the overlocal model and three different mesh spacings. As the plots indicate, the shear band converges to a fixed width with

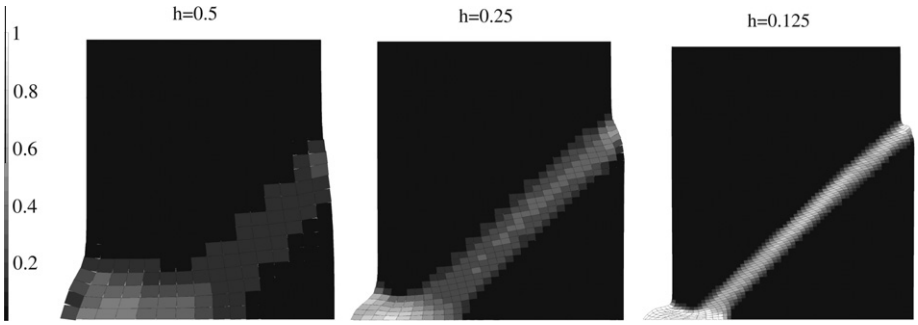

Fig. 2. Contour plot of the magnitude of the plastic strain tensor using a local von Mises plasticity model with isotropic softening. The width of the shear band anomalously reduces with mesh spacing, h.

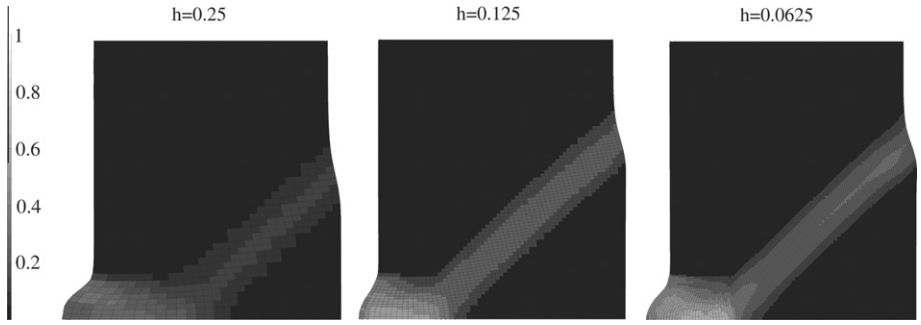

Fig. 4. Contour plot of the magnitude of the plastic strain vector using an overlocal von Mises plasticity model with isotropic softening. With mesh refinement, the width of the shear band converges to a fixed value proportional to the nonlocal length scale.

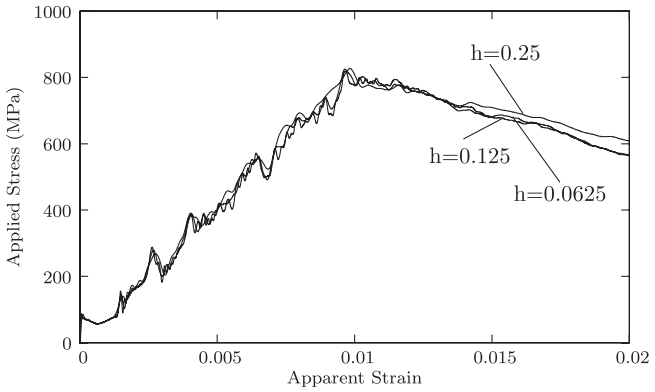

Fig. 5. Plot of the applied stress versus apparent axial strain in the plate using an overlocal von Mises plasticity model and three different mesh resolutions, h, as indicated. With the overlocal model the stress/strain curve converges with mesh refinement.

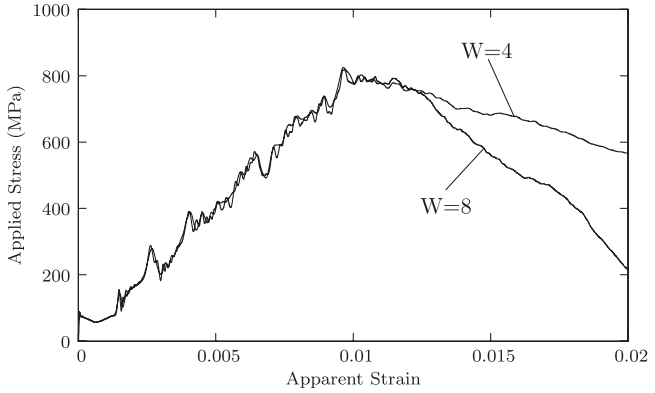

Fig. 6. Plot of the applied stress versus apparent axial strain in the plate using an overlocal von Mises plasticity model and two different plate widths, W, as indicated. All other lengths have been scaled as well so that the two curves are for geometrically similar plates. The difference in the response is due to the size effect that results from nonlocal models.

mesh refinement. The width of the shear band is controlled by the nonlocal length scale.

Unlike the results found using a local model, the overlocal stress–strain curve in Fig. 5 converges with mesh refinement. Specifically, the post-peak stress–strain response is driven by the problem geometry and material parameters rather than by the mesh spacing.

In addition to the convergence of the shear band width to a finite value, nonlocal models also have the advantage of being able

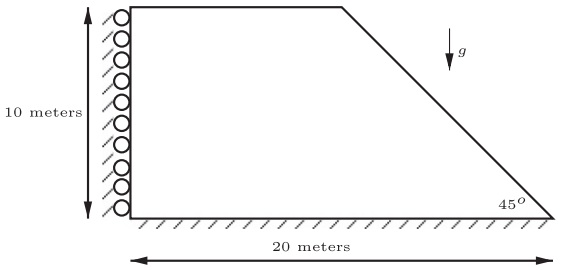

Fig. 7. Schematic of the slope stability problem solved. The lower surface has a fixed boundary condition applied, the surface on the left-hand side has the displacement fixed in the horizontal direction. All other surfaces are traction free. A vertical gravitational field is increased with time at a rate of 4.9 m/s^3. The material is in a state of plane strain.

to capture a size effect. Specifically, two structures of the same shape but different sizes will behave differently under the same applied tractions. With a nonlocal model, the ratio of the length scale associated with the problem geometry to the nonlocal length scale becomes a significant parameter. This is an important characteristic for a model to be capable of predicting large-scale problems based on small-scale laboratory experiments. To illustrate the size effect, the 2D plate case study was also solved using a specimen that is 8 m wide and 10 m high, which is exactly double the size of the original problem. The velocity at the top surface was prescribed to be 15 m/s, which is also exactly double the rate in the previous problem. The result is that the bulk strain rate in the plate is the same as with the original problem. The resulting apparent axial stress versus strain plot, along with that of the original problem, is shown in Fig. 6. Both the original problem and the scaled-up problem were solved with a mesh resolution of $h = 0.25$ m. As the plot indicates, the apparent structural response for the problem with the larger length scale is more brittle than with the original problem. This illustrates the fact that a brittle structural response can result from either a large softening modulus, or from a material micro-structure with a length scale much smaller than the structure's length scale.

6.2. Slope stability problem with Drucker–Prager plasticity model

To demonstrate the use of the nonlocal MPM formulation for frictional materials a slope stability problem is solved using a strain-softening linear Drucker–Prager model. A similar slope stability problem was previously solved by Ortiz et al. [37] using specialized localization elements and by Pamin and de Borst [38] using a gradient plasticity model. As shown in Fig. 7, the problem consists of a 10 m thick, 20 m long rectangular elastoplastic domain. The top surface of the domain is traction free. The bottom

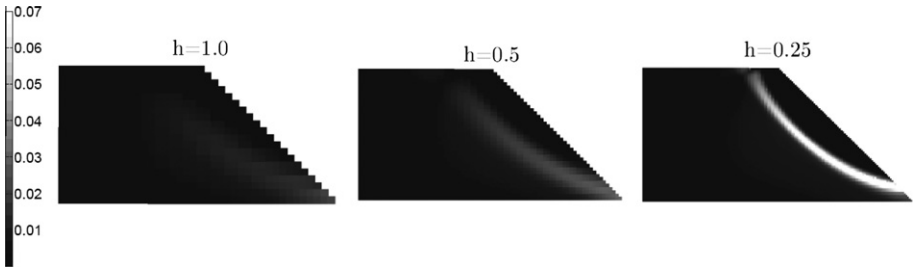

Fig. 8. Contour plot of the magnitude of the plastic strain using a local Drucker–Prager plasticity model with isotropic softening. With mesh refinement, the width of the shear band becomes increasingly small while the magnitude of the plastic strain increases without bound.

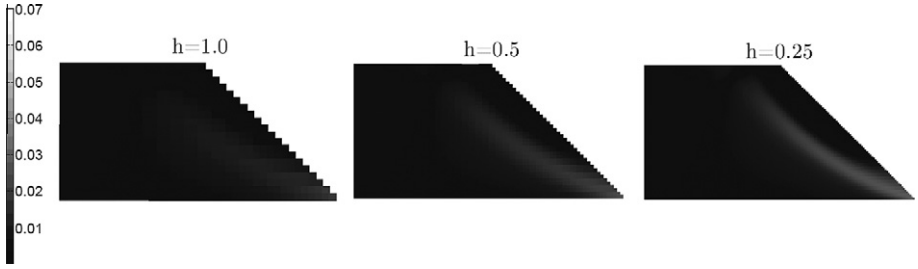

Fig. 9. Contour plot of the magnitude of the plastic strain using an overlocal Drucker–Prager plasticity model with isotropic softening. With mesh refinement both the width of the shear band as well as the magnitude of the plastic strain within the shear band converge to a fixed value.

surface is prescribed to have zero displacement in any direction while the left-hand surface of the domain is prescribed to have zero horizontal displacement, but is free to displace in the vertical direction. As with the previous example, the CPDI formulation of the MPM is used. The bulk modulus is chosen to be 82.7 GPa while the shear modulus is chosen to be 49.6 GPa. A nonassociated Drucker–Prager yield model is used with $\alpha = 0.15$ and $\alpha_p = 0.0$. The problem is first solved using a local linear softening plasticity model with $h_\eta = -689.5$ MPa. The problem is also solved with an overlocal plasticity model with $h_\eta = 1.38$ GPa, $h_\xi = -689.5$ MPa, and a nonlocal length scale of $L = 2$ m.

Fig. 8 shows the plots of the magnitude of the plastic strain field at $t = 2.0$ seconds for three different mesh resolutions with the local plasticity model, while Fig. 9 shows the overlocal solutions at the same time with the same three mesh resolutions. As with the von Mises plasticity example described in the previous section, with the local plasticity model the shear band width becomes increasingly narrow as the mesh is refined and the magnitude of the plastic strain within the shear band becomes increasingly large, and therefore the numerical solution is mesh-dependent. With the overlocal solution the shear band converges to a fixed width and the magnitude of the plastic strain within the shear band also converges to a fixed value, yielding a mesh-independent solution. The width of the shear band with the overlocal model is proportional to the nonlocal length scale. These results are in good agreement with those of Ortiz et al. [37] and Pamin and de Borst [38], though since the regularization approach used in the those works is different from the nonlocal plasticity approach taken here the results would not be expected to be identical.

7. Conclusion

Whereas nonlocal iteration schemes in the literature are typically specialized to apply to a particular choice of yield function, a general framework for deriving a nonlocal iterative solver has been elucidated in this work to apply to any general yield function. Moreover, a straightforward rigorous basis for deriving a corresponding convergence criterion scheme has been here developed using the Banach fixed-point theorem.

While these methods can be applied to any host code framework, they are particularly well suited to incorporation into the material point method (MPM). Specifically, by using the MPM background grid to evaluate the nonlocal integrals, there is no need to maintain a list of particles within the nonlocal neighborhood of a given particle. This attribute not only produces a matrix-free algorithm, but it is especially appealing for large-deformation problems in which the number and identity of material points in the vicinity of any given material point change in time.

References

[1] D. Sulsky, A particle method for history-dependent materials, Comput. Methods Appl. Mech. Engrg. 118 (1–2) (1994) 179, http://dx.doi.org/10.1016/0045-782(94)00033-6.
[2] S. Bardenhagen, E. Kober, The generalized interpolation material point method, Comput. Model. Engrg. Sci. 5 (6) (2004) 477–495.
[3] M. Steffen, P. Wallstedt, J. Guilkey, R. Kirby, M. Berzins, Examination and analysis of implementation choices within the material point method (mpm), CMES – Comput. Model. Engrg. Sci. 31 (2) (2008) 107–127, http://dx.doi.org/10.1002/nme.2360.
[4] J. Guilkey, J. Weiss, Implicit time integration for the material point method: quantitative and algorithmic comparisons with the finite element method, Int. J. Numer. Methods Engrg. 57 (9) (2003) 1323–1338, http://dx.doi.org/10.1002/nme.729.
[5] D. Sulsky, A. Kaul, Implicit dynamics in the material-point method, Comput. Methods Appl. Mech. Engrg. 193 (12–14) (2004) 1137–1170, http://dx.doi.org/10.1016/j.cma.2003.12.011.
[6] A. York, D. Sulsky, H. Schreyer, The material point method for simulation of thin membranes, Int. J. Numer. Methods Engrg. 44 (1999) 1429–1456.
[7] E. Love, D. Sulsky, An energy-consistent material-point method for dynamic finite deformation plasticity, Int. J. Numer. Methods Engrg. 65 (2005) 1608–1638.
[8] J. Nairn, Material point method calculations with explicit cracks, Comput. Model. Engrg. Sci. 4 (2003) 649–663.
[9] Y. Guo, J. Nairn, Three-dimensional dynamic fracture analysis using the material point method, Comput. Model. Engrg. Sci. 16 (2006) 141–155.
[10] S. Ma, X. Zhang, X. Qiu, Comparison study of mpm and sph in modeling hypervelocity impact problems, Int. J. Impact Engrg. 36 (2009) 272–282.
[11] J. Burghardt, B. Leavy, J. Guilkey, Z. Xue, R. Brannon, Application of uintah-mpm to shaped charge jet penetration of aluminum, IOP Conference Series: Materials Science and Engineering, vol. 10, 2010, p. 012223 (9 pp.). http://dx.doi.org/10.1088/1757-899X/10/1/012223.
[12] Z.P. Bažant, A. Zubelewicz, Strain-softening bar and beam: exact non-local solution, Int. J. Solids Struct. 7 (7) (1988) 659–673.

[13] R. de Borst, L. Sluys, H. Muhlhaus, J. Pamin, Fundamental issues in finite element analyses of localization of deformation, Engrg. Comput. 10 (1993) 99–121.
[14] A.C. Erigen, On nonlocal plasticity, Int. J. Engrg. Sci. 19 (1981) 1461–1474.
[15] Z.P. Bažant, F.-B. Lin, Non-local yield limit degradation, Int. J. Numer. Methods Engrg. 26 (1988) 1805–1823.
[16] T. Belytschko, M. Kulkarni, On imperfections and spatial gradient regularization in strain softening viscoplasticity, in: Failure criteria and analysis in dynamic response, presented at the Winter Annual Meeting of the American Society of Mechanical Engineers, vol. 107, Dallas, TX, USA, 1990, pp. 1–5.
[17] E. Aifantis, Strain gradient interpretation of size effects, Int. J. Fract. 95 (1999) 299–314.
[18] Z.P. Bažant, S.-D. Pang, Activation energy based extreme value statistics and size effect in brittle and quasibrittle fracture, J. Mech. Phys. Solids 55 (1) (2007) 91–131, http://dx.doi.org/10.1016/j.jmps.2006.05.007.
[19] R.A. Engelen, M.G. Geers, F.P. Baaijens, Nonlocal implicit gradient-enhanced elastoplasticity for the modeling of softening behavior, Int. J. Plast. 19 (2003) 403–433.
[20] M. Geers, Finite strain logarithmic hyperelasto-plasticity with softening: a strongly non-local implicit gradient framework, Comput. Methods Appl. Mech. Engrg. 193 (30–32) (2004) 3377, http://dx.doi.org/10.1016/j.cma.2003.07.014.
[21] R. De Borst, H.-B. Muehlhaus, Gradient-dependent plasticity: formulation and algorithmic aspects, Int. J. Numer. Methods Engrg. 35 (3) (1992) 521–539.
[22] R. Peerlings, M. Geers, R. de Borst, W. Brekelmans, A critical comparison of nonlocal and gradient-enhanced softening continua, Int. J. Solids Struct. 38 (2001) 7723–7746.
[23] Z.P. Bažant, M. Jirasek, Nonlocal integral formulations of plasticity and damage: survey of progress, J. Engrg. Mech. 128 (2002) 1119–1149. <http://dx.doi.org/10.1061/*ASCE*0733-9399*2002*128:11*1119*>.
[24] G. Di Luzio, Z. Bažant, Spectral analysis of localization in nonlocal and over-nonlocal materials with softening plasticity or damage, Int. J. Solids Struct. 42 (23) (2005) 6071–6100, http://dx.doi.org/10.1016/j.ijsolstr.2005.03.038.
[25] L. Stromberg, M. Ristinmaa, Fe-formulation of a nonlocal plasticity theory, Comput. Methods Appl. Mech. Engrg. 136 (1996) 124–144.
[26] J.-S. Chen, C.-T. Wu, T. Belytschko, Regularization of material instabilities by meshfree approximations with intrinsic length scales, Int. J. Numer. Methods Engrg. 47 (7) (2000) 1303–1322.
[27] X. Pan, H. Yuan, Nonlocal damage modelling using the element-free Galerkin method in the frame of finite strains, Comput. Mater. Sci. 46 (3) (2009) 660–666, http://dx.doi.org/10.1016/j.commatsci.2009.03.044.
[28] O. Weckner, S. Silling, A. Askari, Dispersive wave propagation in the nonlocal peridynamic theory, in: Proceedings of the ASME International Mechanical Engineering Congress and Exposition, vol. 12, Boston, MA, United states, 2009, pp. 503–504.
[29] A. Sadeghirad, R.M. Brannon, J. Burghardt, A convected particle domain interpolation technique to extend applicability of the material point method for problems involving massive deformations, Int. J. Numer. Methods Engrg. 86 (12) (2011) 1435–1456, http://dx.doi.org/10.1002/nme.3110.
[30] P. Wallstedt, J. Guilkey, An evaluation of explicit time integration schemes for use with the generalized interpolation material point method, J. Comput. Phys. 227 (22) (2008) 9628–9642, http://dx.doi.org/10.1016/j.jcp.2008.07.019.
[31] P. Wallstedt, J. Guilkey, Improved velocity projection for the material point method, CMES – Comput Model. Engrg. Sci. 19 (3) (2007) 223–232.
[32] M. Jirasek, S. Rolshoven, Comparison of integral-type nonlocal plasticity models for strain-softening materials, Int. J. Engrg. Sci. 41 (13–14) (2003) 1553–1602, http://dx.doi.org/10.1016/S0020-722(03)00027-2.
[33] J.M. Ortega, W.C. Rheinboldt, Iterative Solution of Nonlinear Equations in Several Variables, Society for Industrial and Applied Mathematics, Philadelphia, PA, USA, 2000.
[34] J. Simó, T. Hughes, Computational Inelasticity, Interdisciplinary Applied Mathematics: Mechanics and Materials, Springer, 1998.
[35] J. de St. Germain, J. McCorquodale, S. Parker, C. Johnson, Uintah: a massively parallel problem solving environment, Ninth IEEE International Symposium on High Performance and Distributed Computing, vol. 41, IEEE, Piscataway, NJ, 2000, p. 33. <http://www.sci.utah.edu/publications/dav00/uintah-hpdc00.pdf>.
[36] Z.P. Bažant, Instability, ductility, and size effect in strain-softening concrete, ASCE J. Engrg. Mech. Div. 102 (2) (1976) 331–344.
[37] M. Ortiz, Y. Leroy, A. Needleman, A finite element method for localized failure analysis, Comput. Methods Appl. Mech. Engrg. 61 (1987) 198–214.
[38] J. Pamin, R. de Borst, Numerical simulation of localization phenomena using gradient plasticity, Heron 1 (1995) 71–92, TNO Built Environment and Geosciences, Delft, and the Netherlands School for Advanced Studies in Construction.